ARTICLES
PUBLISHED ONLINE: 20 SEPTEMBER 2009 | DOI: 10.1038/NPHYS1396
nature physics

Topology-driven quantum phase transitions in time-reversal-invariant anyonic quantum liquids

Charlotte Gils[1], Simon Trebst[2]*, Alexei Kitaev[3], Andreas W. W. Ludwig[4], Matthias Troyer[1] and Zhenghan Wang[2]

Indistinguishable particles in two dimensions can be characterized by anyonic quantum statistics, which is more general than that of bosons or fermions. Anyons emerge as quasiparticles in fractional quantum Hall states and in certain frustrated quantum magnets. Quantum liquids of anyons show degenerate ground states, where the degeneracy depends on the topology of the underlying surface. Here, we present a new type of continuous quantum phase transition in such anyonic quantum liquids, which is driven by quantum fluctuations of the topology. The critical state connecting two anyonic liquids on surfaces with different topologies is reminiscent of the notion of a 'quantum foam' with fluctuations on all length scales. This exotic quantum phase transition arises in a microscopic model of interacting anyons for which we present an exact solution in a linear geometry. We introduce an intuitive physical picture of this model that unifies string nets and loop gases, and provide a simple description of topological quantum phases and their phase transitions.

Phases of matter can show a vast variety of ordered states that typically arise from spontaneous symmetry breaking and can be described by a local order parameter. A more elusive form of order known as 'topological order'[1] reveals itself through the appearance of robust ground-state degeneracies, but cannot be described in terms of a local order parameter. Examples of such topological quantum liquids are the fractional quantum Hall states[2] where the ground-state degeneracy depends on the number of 'antidots', which can be viewed as punctures (holes) in the two-dimensional surface populated by the quantum Hall liquid[3]. It has long been proposed that topological quantum liquids also occur in certain frustrated quantum magnets[4–9], but it has only been in recent years that strong candidate materials have emerged[10,11]. Whereas quantum Hall liquids break time-reversal symmetry, the exotic ground states of frustrated quantum magnets are expected to preserve time-reversal symmetry. As a consequence of this symmetry, many unexplored phenomena may appear, including the intriguing possibility of topology-driven quantum phase transitions, which is the central aspect of this article.

In this article, we develop an intuitive physical picture for the emerging low-energy physics of topological quantum liquids and their phase transitions in terms of surfaces and their topology. We thereby provide a visualization of the underlying quantum physics, which is in one-to-one correspondence with a detailed analytical framework. Here, we consider systems that preserve time-reversal symmetry, which in this picture will be described by quantum liquids on closed surfaces or by two sheets of quantum liquids with opposing chirality—so-called quantum doubles. Such liquids show ground-state degeneracies that depend (exponentially) on the genus of the surface. A section of an extended high-genus surface formed by a triangular arrangement of 'holes' is shown in Fig. 1. Through every such hole there can be a flux of the liquid populating the surface. An exponential degeneracy then arises from the possible flux assignments through the holes. Whereas in the presence of a flux a hole cannot be contracted, we can eliminate the hole in the absence of flux without changing the state of the topological liquid. If there is no flux through any of the holes, they can all be removed, and the state of the quantum liquid is identical to that on two separated sheets, as shown on the left-hand side of Fig. 1. It is this state that shows topological order. On the other hand, if there is no flux through the tubes in the interior of the surface (centred around the black lines in Fig. 2), we can pinch them off. The resulting state of the quantum liquid is then identical to that of disconnected spheres, as shown on the right-hand side of Fig. 1. This state has neither ground-state degeneracy nor topological order.

Quantum doubles, string nets and competing topologies

Here we will introduce a microscopic model that energetically favours the absence of flux through the holes or tubes, thus dynamically implementing the two topology-changing processes mentioned above. The competition of the two processes drives a quantum phase transition between the two extreme states. Our model is defined on the 'skeleton' that surrounds the holes in the interior of the surface, as illustrated in Fig. 2a, where the skeleton forms a honeycomb lattice. The fluxes in the tubes are associated with discrete degrees of freedom on the edges of the skeleton lattice, corresponding to anyonic particles[12] of the quantum liquid. The set of degenerate ground states of the liquid is now in one-to-one correspondence with all labellings of the edges consistent with a given set of constraints, characteristic of the underlying quantum liquid.

As a simple example, we consider a quantum liquid of so-called Fibonacci anyons[13–15]. Here there are only two possible labellings, namely the trivial particle **1** and the Fibonacci anyon τ. At any trivalent vertex of the skeleton lattice, there is a constraint forbidding the appearance of only a single τ-anyon on the three edges connected to the vertex, allowing the following possibilities shown in Fig. 3.

[1]Theoretische Physik, ETH Zurich, 8093 Zurich, Switzerland, [2]Microsoft Research, Station Q, University of California, Santa Barbara, California 93106, USA, [3]Institute for Quantum Information, California Institute of Technology, Pasadena, California 91125, USA, [4]Department of Physics, University of California, Santa Barbara, California 93106, USA. *e-mail: trebst@kitp.ucsb.edu.

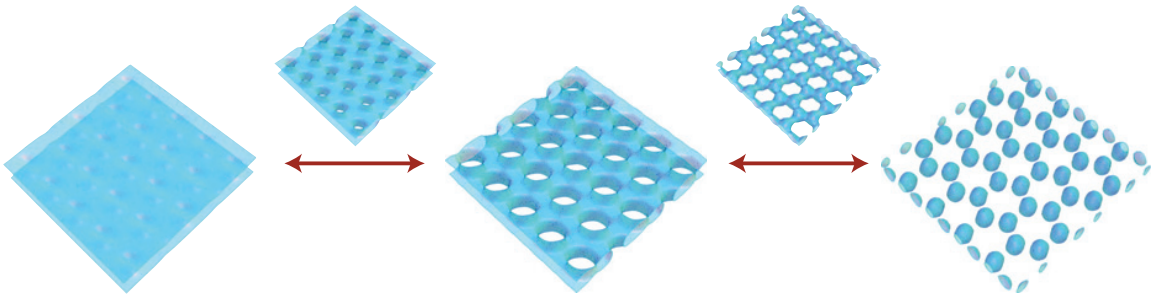

Figure 1 | Phase transition in two dimensions. Two-dimensional surfaces with different topologies that are populated by anyonic quantum liquids. A quantum phase transition driven by fluctuations of the surface topology connects the anyonic liquid with topological order on two separated sheets (on the left) and the anyonic liquid without topological order on decoupled spheres (on the right).

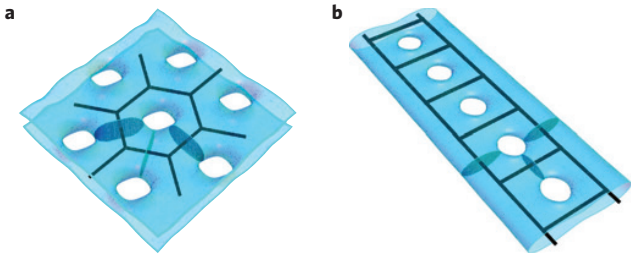

Figure 2 | Microscopic model. Our microscopic model energetically favours the flux-free states for the holes and tubes (shaded) of the illustrated two-dimensional surfaces. **a**, For the surface with a triangular arrangement of holes, the anyonic degrees of freedom in our model are associated with the edges of the honeycomb skeleton lattice that surrounds the holes in the interior of the surface. **b**, For the linear geometry of holes, the skeleton lattice forms a ladder geometry.

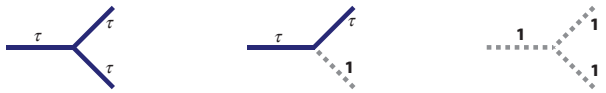

Figure 3 | The Fibonacci theory. The allowed labellings at a trivalent vertex in the Fibonacci theory.

Owing to this constraint, the edges occupied by a τ-anyon form a closed, trivalent net known as a 'string net'[7]. One might as well identify the two degrees of freedom $(\mathbf{1}, \tau)$ with the two states of a pseduo-spin $(\uparrow, \downarrow)$ and thus the same states can be viewed as representing the ground states of a Hamiltonian with three-spin interactions enforcing the vertex constraint above (no single $\downarrow$-spin around a vertex)[16].

Returning to our model, we can now specify its microscopic terms

$$H = -J_e \sum_{\text{edges } e} \delta_{\ell(e),\mathbf{1}} - J_p \sum_{\text{plaquettes } p} \delta_{\phi(p),\mathbf{1}} \qquad (1)$$

The first term favours a trivial label $\ell(e) = \mathbf{1}$ on the edge e corresponding to the no-flux state. The second term favours the no-flux state $\phi(p) = \mathbf{1}$ for the plaquette p. When expressed in terms of the labels $\ell(e)$, the plaquette flux $\phi(p)$ is a complicated, but local expression involving the 12 edges connected to the vertices surrounding a plaquette, see Fig. 2, and is explicitly given in the Supplementary Information. In the absence of the first term ($J_e = 0$), the plaquette term with $J_p > 0$ will effectively close all holes, and the ground state of the above Hamiltonian describes that of the quantum liquid on two parallel sheets, as illustrated in Fig. 1. This second case is precisely the string-net model first introduced by Levin and Wen[7], which is also closely related to another model of string nets discussed recently by Fendley[17]. Similarly, in the absence of the plaquette term, $J_p = 0$, the edge term with coupling constant $J_e > 0$ will close off all of the 'tubes', thus leading to the ground state of the quantum liquid on multiple disconnected spheres, as illustrated in Fig. 1. This edge term acts as a string tension in the string-net model, or as a magnetic field in its pseudo-spin representation.

In the presence of both terms in the Hamiltonian, quantum fluctuations are introduced that correspond to fluctuations of the surface. These fluctuations are virtual processes where plaquettes or tubes close off and open depending on the flux through them. We can visualize these fluctuations as local changes to the genus of the surface. If the two terms in the Hamiltonian become comparable in strength, the competition between the two drives a quantum phase transition between the two extremal topologies (see Fig. 1). At this quantum phase transition, the fluctuations of the surface become critical and the topology of the surface fluctuates on all length scales. We can visualize the (imaginary) time evolution of this quantum critical state as a 'foam' in spacetime, which is reminiscent of the notion of a quantum foam introduced by Wheeler for fluctuations of 3+1 dimensional Minkowski space at the Planck scale[18,19].

Phase transitions and exact solution in linear geometry

To understand the nature of this transition, we first focus on the linear geometry shown in Fig. 2b. In this geometry, the Hamiltonian becomes

$$H = -J_r \sum_{\text{rungs } r} \delta_{\ell(r),\mathbf{1}} - J_p \sum_{\text{plaquettes } p} \delta_{\phi(p),\mathbf{1}} \qquad (2)$$

where the first term now acts only on the rungs between the holes (that is, on those edges of the skeleton that separate two neighbouring plaquettes), in analogy to the original model. This model shows a continuous quantum phase transition between the two extreme topologies shown in Fig. 4. This continuous transition is driven by fluctuations of topology. It turns out that the gapless theory describing this transition can be solved exactly, as discussed in more detail below and explicitly in the Supplementary Information.

The two extreme topologies connected by this transition in the linear geometry are as follows. In the limit of a vanishing rung term, $J_r = 0$, the ground state is that of an anyonic quantum liquid on a single cylinder where all of the plaquettes are closed, as shown on the left in Fig. 4. For Fibonacci anyons, this ground state is two-fold degenerate, with either a τ-flux or no flux through the cylinder. In the opposite limit of vanishing plaquette term, $J_p = 0$, we can close off all of the rungs and the ladder splits into two separate cylinders with a four-fold ground-state degeneracy (either a τ-flux or no flux in either of the cylinders), as shown on the right in Fig. 4.

In both limits, excitations above these ground states are gapped quasiparticles with a gap of J_p or J_r, respectively. The first excited

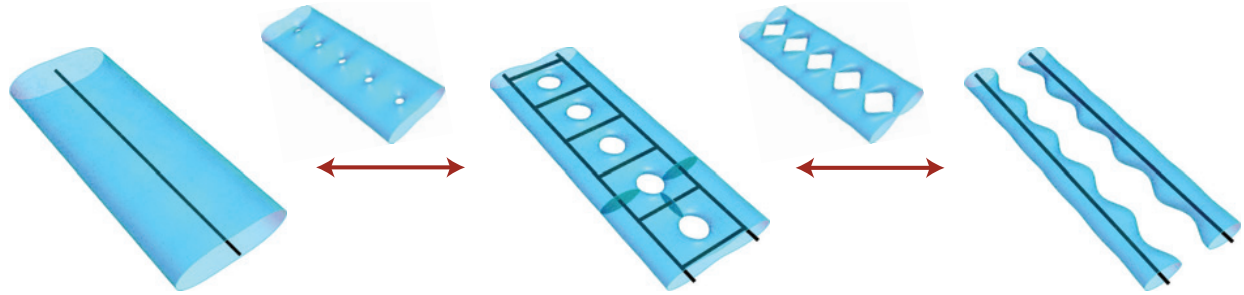

Figure 4 | Phase transition in one dimension. Illustration of the quantum phase transition driven by fluctuations of the surface topology in a linear geometry that connects the extreme limits of a single cylinder (on the left) and two cylinders (on the right).

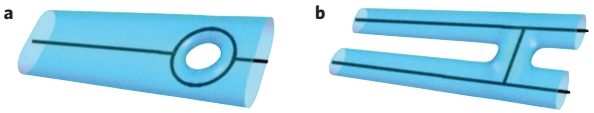

Figure 5 | Excitations of the ladder model. a,**b**, Plaquette (**a**) and rung (**b**) excitations above the two extreme ground states illustrated in Fig. 4.

state above the 'single cylinder' ground state is a τ-flux threading a single plaquette, which prevents it from being closed, as illustrated in Fig. 5a. In the opposite limit of the 'two cylinder' ground state, the first excited state is a τ-flux through one of the rungs, leaving this rung connecting the two cylinders as shown in Fig. 5b. Turning on a small coupling $J_r \neq 0$, or $J_p \neq 0$ respectively, these excitations delocalize, but remain gapped and form bands in the energy spectrum, as explicitly shown in Fig. 6a. For large couplings, some of these excitations proliferate and their gap vanishes at the quantum phase transition mentioned above.

The full phase diagram is shown in Fig. 6b, where we parameterize the two couplings on a circle as $J_p = \cos\theta$ and $J_r = \sin\theta$. Positive (negative) coupling constants indicate that the no-flux (τ-flux) states are energetically favoured and the two extreme limits discussed above then correspond to the points $\theta = 0$ and $\theta = \pi/2$ on the circle. The continuous phase transition between these two distinct topologies occurs for equal positive coupling strengths $J_r = J_p$, which corresponds to the point $\theta = \pi/4$ on the circle.

We can visualize this critical point as a quasi-one-dimensional quantum foam, with topology fluctuations of the surface on all length scales. As a first step, we have carried out a detailed numerical analysis of this critical point using exact diagonalization of systems with up to 36 anyons. The continuous nature of the phase transition reveals itself in a linear energy–momentum dispersion relationship, which is indicative of conformal invariance. A detailed analysis of the energy spectrum further allows us to uniquely identify the corresponding conformal field theory (CFT), which in this case turns out to be the seventh member of the famous series of so-called unitary minimal CFTs (ref. 20) with central charge $c = 14/15$ (more specifically, the 'non-diagonal modular invariant'[21]). This particular identification of a CFT is part of a broader scheme that connects the gapless theory of the topology-driven phase transition with the nature of the underlying anyonic liquid. In the present case of a quantum liquid of Fibonacci anyons, we can make an explicit connection between the (total) quantum dimension of the anyonic liquid and the central charge of the conformal field theory.

In fact, the Hamiltonian at this point is even exactly solvable. The key insight leading to this exact, analytical solution is the observation that the Hamiltonian of our topological model can be mapped precisely onto a particular version of the restricted-solid-on-solid (RSOS) model[22], which is exactly integrable and directly leads to the above-mentioned CFT. This mapping explicitly connects the Hamiltonian at this critical point with an integrable Hamiltonian defined by the Dynkin diagram D_6 shown in Fig. 7. Here, the particular labelling of the Dynkin diagram arises from the underlying topological structure of our model. Specifically, the labels describe the topological fluxes in the two extreme limits of the model, as illustrated in Fig. 4, with the limit of a single cylinder in the picture on the left corresponding to the blue circles in the Dynkin diagram and the limit of the two cylinders pictured on the right corresponding to the green circles. This underlying structure also gives rise[23] to a representation of the Temperley–Lieb algebra[24], which is characterized by the total quantum dimension $D = \sqrt{2+\phi}$ of the anyonic liquid, where $\phi = (1+\sqrt{5})/2$ is the golden ratio. A more detailed discussion of the exact solution is given in the Methods section and the Supplementary Information.

Varying the couplings in our Hamiltonian, there is another way of connecting the two phases shown in Fig. 4, which is to change the sign of both couplings in the Hamiltonian. For opposite sign, the two terms now favour τ-fluxes through rungs and plaquettes, respectively, which again leads to a competition. Interestingly, we find that this competition results in an extended, critical phase separating the two topologically distinct phases, as shown in the phase diagram of Fig. 6b. For the full extent of this critical phase we again have topology fluctuations on all length scales. However, the gapless theory describing this phase turns out to be in a different universality class as compared with the critical point discussed above. These results can again be obtained through a combination of numerical and exact analytical arguments, which are detailed in the Supplementary Information. In particular, there is another integrable point in this extended critical phase for equal coupling strengths $J_r = J_p$, which corresponds to the angle $\theta = 5\pi/4$ in the phase diagram of Fig. 6b, and is thus located exactly opposite to the one discussed above. Following a similar route, one can map the Hamiltonian at this second integrable point to another variant of the RSOS model associated with the Dynkin diagram D_6. The gapless theory at this point then turns out to be exactly the Z_8 parafermion CFT with central charge $c = 7/5$. The stability of this gapless theory away from the integrable point is due to an extra symmetry of our model[25,26]. Numerically, we find that it extends throughout the whole region where both couplings favour the τ-flux states all the way to the points $\theta = \pi$ and $\theta = 3\pi/2$, where there is no longer a competition of the two terms of the Hamiltonian and the ground states have fluxes either through all plaquettes or rungs, respectively.

Semions and loop gases in two dimensions

Returning to our original discussion of the two-dimensional model (1) on the surface in Fig. 1, the question arises whether we can understand the nature of the quantum phase transition here as well. We can explicitly address this question in the context of another kind of anyons, the so-called semions[27]. Again, there are two possible labellings, the trivial particle **1** and the semion s. The constraint now only allows zero or two semion particles s at any trivalent vertex. The set of edges carrying a semion s form loops

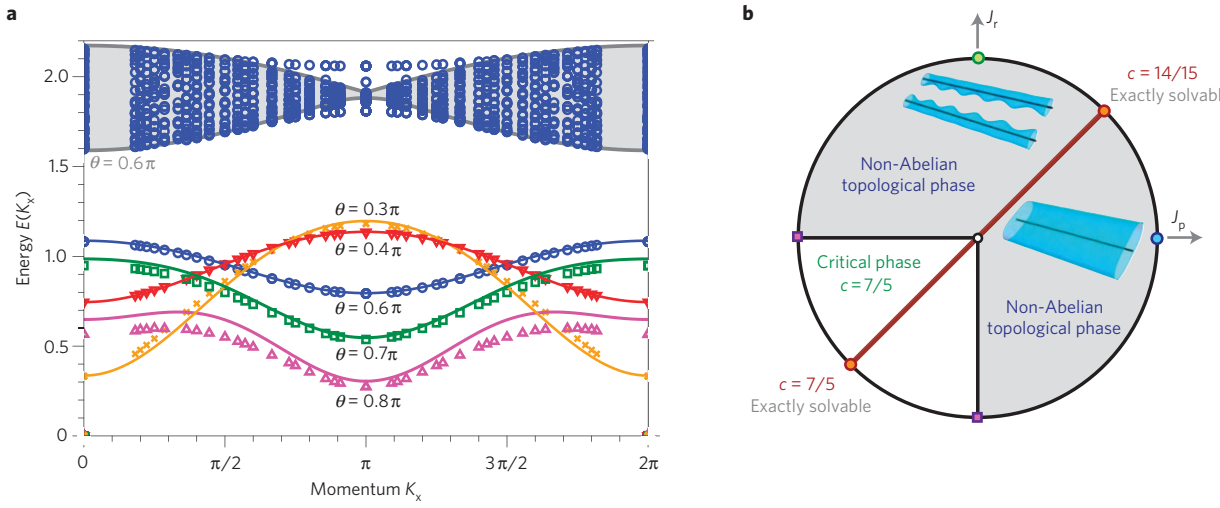

Figure 6 | Energy spectra and phase diagram. a, Energy spectra of our microscopic model near the decoupling point ($\theta = \pi/2$). The rung excitations shown in Fig. 5 form a gapped quasiparticle band well below a continuum of states (shaded). Open symbols show results from exact diagonalization of systems with 24 to 36 anyons. These bands are well described by second-order perturbation theory around the decoupling point shown as solid lines. **b**, The phase diagram of our microscopic model (2) where the couplings are parametrized as $J_p = \cos\theta$ and $J_r = \sin\theta$. The gapped topological phases are indicated by the shaded regions. The topology-driven quantum phase transition occurs at the exactly solvable critical point $\theta = \pi/4$. An extended critical phase is found in the region $\theta \in (\pi, 3\pi/2)$ around the second solvable (critical) point $\theta = 5\pi/4$. Both critical states correspond to the quantum foam picture discussed in the text.

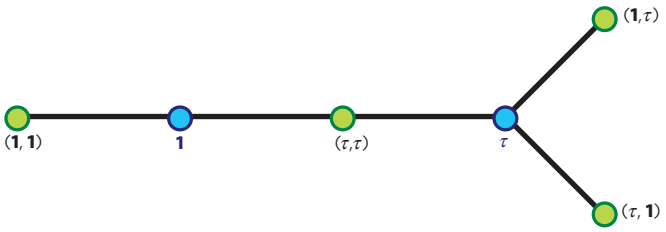

Figure 7 | The D_6 Dynkin diagram. The integrable Hamiltonian at the solvable points in the phase diagram can be mapped onto this diagram.

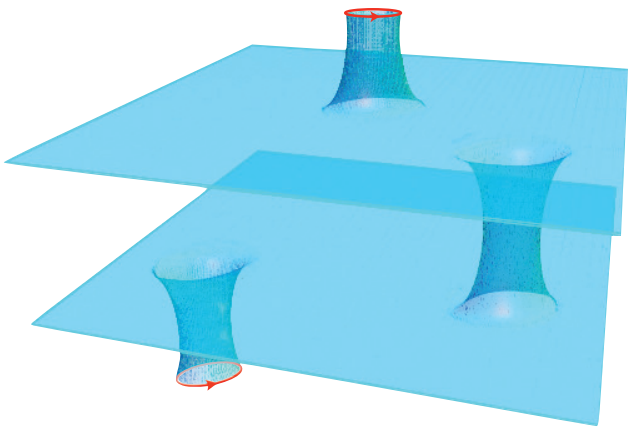

Figure 8 | Excitations of the anyonic liquid. Vortex excitations of the liquid indicated by the 'chimneys' possess a chiral edge mode.

instead of nets and give rise to what is known as a loop gas[8,28]. In a pseudo-spin representation (where $\uparrow, \downarrow$ now stand for **1** and s), this model is known as the honeycomb version of the toric code[8], where the string tension J_e corresponds to a magnetic field. This model shows a continuous quantum phase transition in the three-dimensional Ising universality class[29,30] with topology fluctuations on all length scales. Mapping the 2+1 dimensional semion system to its three-dimensional classical counterpart, the quantum foam then corresponds to the critical fluctuations of domain walls in a three-dimensional Ising model at its critical point. For other kinds of anyonic liquids, the nature of the topology-changing transition is in general unknown and remains an intriguing open problem with the possibility of new universality classes. For a liquid of Fibonacci anyons, there has been a recent discussion of quantum critical behaviour from the perspective of ground-state wavefunctions and their respective correlators in terms of conformal field theory[17,31].

Chimneys, holes and chirality

Finally, to explore the broader context of our models, we complete our analysis by considering the complete set of possible excitations present in these models. An excitation different from the ones already discussed arises when relaxing the constraint that for every trivalent vertex of the skeleton lattice forbids the occurrence of a single τ-flux. If we allow for this possibility, we are left with a τ-flux entering the vertex through one tube, but not leaving it through another tube in the skeleton plane, as illustrated in Fig. 2. Instead, we can think of the remaining τ-flux at such a vertex as leaving through one of the liquid sheets surrounding the skeleton lattice. This piercing of the liquid by a τ-flux corresponds to a vortex excitation of the liquid and is illustrated as a 'chimney' in Fig. 8. These vortex excitations break time-reversal symmetry and turn out to all possess the same chirality (indicated by the red arrow in Fig. 8). This is possible only if the anyonic liquid on a given sheet itself possesses a given chirality. As the entire system shows time-reversal symmetry, this means that the two anyonic liquids on the two sheets must have opposite chirality. Vortices associated with chimneys on opposite sheets thus also have opposite chirality, as illustrated in Fig. 8. (In fact, a vortex in one sheet can be related to a vortex in the opposite sheet by dragging a vortex through a 'hole' connecting the two sheets. Moreover, we can create a 'hole' connecting the sheets by gluing together two vortex excitations on opposite sheets.) This conceptual perspective of two anyonic liquids with opposite chirality giving rise to a time-reversal-invariant model connects with and allows for a visualization of a more abstract mathematical description of these models, namely doubled non-Abelian Chern–Simons theories[32] and their lattice regularization in terms of string nets.

A unifying framework

Our construction of time-reversal-invariant quantum double models provides a unifying framework for a large class of anyon theories, going beyond that of semions and Fibonacci anyons. This framework extends to topological phases and phase transitions for anyon theories with an arbitrary number of anyons subject to a set of fusion rules/constraints that correspond to more complex string nets, as outlined in the Supplementary Information. We expect this framework to be a natural description of topological spin-liquid states and their phase transitions in frustrated quantum magnets and other time-reversal-invariant strongly correlated systems. Quantum phase transitions between topological phases have so far been largely unexplored territory, especially from the perspective of conventional Landau–Ginzburg–Wilson theory, and it remains an intriguing question to formulate our topology-driven phase transitions within such a field theoretical perspective. Even when the topology-driven quantum phase transition in two spatial dimensions is first order, we note that disorder will round off the transition such that it becomes continuous as rigorously established in a recent theorem by Greenblatt and collaborators[33]. Thus, these two-dimensional quantum phase transitions will generically show topology fluctuations on all length scales in the presence of disorder.

Methods

Identification of CFTs. To characterize the CFT of the critical points in the linear (ladder) geometry, we rescale and match the finite-size energy spectra obtained numerically by exact diagonalization for systems with up to $L = 36$ anyons to the form of the spectrum of a CFT,

$$E = E_1 L + \frac{2\pi v}{L}\left(-\frac{c}{12} + h + \bar{h}\right) \tag{3}$$

where the velocity v is an overall scale factor and c is the central charge of the CFT. The scaling dimensions $h+\bar{h}$ take the form $h = h^0 + n$, $\bar{h} = \bar{h}^0 + \bar{n}$, where n and $\bar{n}$ are non-negative integers and h^0 and $\bar{h}^0$ are the holomorphic and antiholomorphic conformal weights of primary fields in a given CFT with central charge c. The momenta (in units $2\pi/L$) are such that $k_x = h - \bar{h}$ or $k_x = h - \bar{h} + L/2$. Using this procedure, we find that for the critical point at $\theta = \pi/4$, the rescaled energy spectrum matches the assignments (3) of the non-diagonal modular invariant[21] of the seventh member of the famous series of unitary minimal CFTs[20] with central charge $c = 14/15$. Similarly, at the point $\theta = 5\pi/4$, we find the rescaled energy spectrum to match that of the Z_8 parafermion CFT with central charge $c = 7/5$. For the calculated energy spectra and the details of these assignments, see Supplementary Information.

Exact analytical solution. The Hamiltonian in equation (2) can be solved exactly for interaction strengths corresponding to angles $\theta = \pi/4$ and $\theta = 5\pi/4$ in the phase diagram of Fig. 6b. This exact, analytical solution of the gapless theories at these points unambiguously demonstrates the continuous nature of the related quantum phase transitions and points to generalizations of these gapless theories for other kinds of anyonic liquids. The key observation underlying this exact solution is the emergence of the D_6 Dynkin diagram from the topology of the surface associated with the ladder model as shown in Fig. 2b. Each labelling of the edges of the 'skeleton' graph that corresponds to that surface denotes one of the states spanning the Hilbert space of the system. A crucial step is to consider a different 'pants decomposition'[34] of this surface and to carry out a basis change to a new basis that corresponds to the labelling of the skeleton lattice of this alternative pants decomposition. Explicitly, this basis transformation can be written as

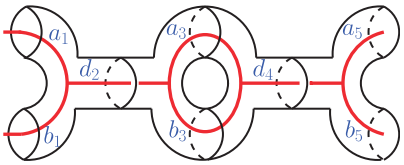

$$= \sum_{c2,c4} (F^{b_3}_{b_1 a_1 a_3})^{c_2}_{d_2} \quad (F^{b_5}_{b_3 a_3 a_5})^{c_4}_{d_4}$$

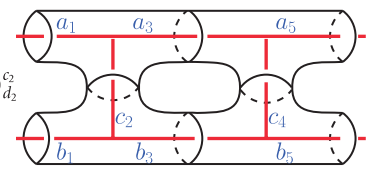

Here, $(F^a_{bcd})^{b'}_{a'}$ denotes the so-called F-matrix, which is a generalization of the familiar $6j$ symbols of angular momentum coupling in conventional quantum mechanics and is known for any anyonic liquid[35]. Note that associated with the even-numbered indices of these labels, which correspond to the original rung labels c_i on the right, there is the flux through the cross-section of the surface on the left, denoted by a label $d_i = \mathbf{1}$ or $d_i = \tau$. Similarly, associated with the odd-numbered indices, which correspond to the original plaquettes, there is a pair of fluxes through the two cross-sections of the surface at the position of the plaquette on the left, denoted by a pair of labels, (a_i, b_i). This pair of labels can assume four values, that is, $(a_i, b_i) = \{(\mathbf{1},\mathbf{1});(\tau,\mathbf{1});(\mathbf{1},\tau);(\tau,\tau)\}$. The (fusion) constraints at the vertices where the labels (a_i, b_i) and $d_{i\pm1}$ meet then turn out to be precisely the condition that they be adjacent nodes on the D_6 Dynkin diagram shown in Fig. 7. For example, only a local label $(a_i, b_i) = (\tau,\tau)$ at an odd-numbered index i allows for either of the two labels $d_{i-1} = \mathbf{1}$ or $d_{i-1} = \tau$ to appear at the neighbouring even-numbered index. This is reflected in the Dynkin diagram by the appearance of a line that connects the label (τ,τ) to both labels $\mathbf{1}$ and τ. The importance of the just-described basis change consists of the fact that in the new basis the rung and plaquette terms, H^{r}_i and H^{p}_i, respectively, of our ladder Hamiltonian

$$H = -J_{\mathrm{r}} \sum_{i\,\mathrm{even}} H^{\mathrm{r}}_i - J_{\mathrm{p}} \sum_{i\,\mathrm{odd}} H^{\mathrm{p}}_i$$

turn out to have precisely the form of a known representation[23] of the Temperley–Lieb algebra[24] associated with the D_6 Dynkin diagram,

$$\mathbf{e}_i^2 = D\,\mathbf{e}_i, \quad \mathbf{e}_i \mathbf{e}_{i\pm1} \mathbf{e}_i = \mathbf{e}_i, \quad [\mathbf{e}_i, \mathbf{e}_j] = 0 \quad \text{for } |i-j| \geq 2$$

where

$$\mathbf{e}_i = \begin{cases} D\,H^{\mathrm{r}}_i & \text{for } i \text{ even} \\ D\,H^{\mathrm{p}}_i & \text{for } i \text{ odd} \end{cases}$$

The characteristic 'D-isotopy' parameter of this Temperley–Lieb algebra, $D = \sqrt{1+\varphi^2} = 2\cos(\pi/10)$, is precisely the total quantum dimension of the underlying Fibonacci anyon liquid. We have thereby established a remarkable, explicit connection of the one parameter of this emerging algebraic structure, the 'D-isotopy' parameter of this Temperley–Lieb algebra, and the single most characteristic parameter of the underlying anyonic liquid, namely its total quantum dimension. This observation points to a generalization of such a connection for other quantum liquids. Written in this form, the resulting Hamiltonian for the Fibonacci anyon liquid turns out to be precisely that of the (integrable) RSOS statistical mechanics lattice model based on the D_6 Dynkin diagram[23], as obtained in the standard fashion from the transfer matrix of the RSOS lattice model. For further details, see Supplementary Information.

Received 18 September 2008; accepted 13 August 2009; published online 20 September 2009

References

1. Wen, X.-G. Vacuum degeneracy of chiral spin states in compactified space. *Phys. Rev. B* **40,** 7387–7390 (1989).
2. Laughlin, R. B. Anomalous quantum Hall effect: An incompressible quantum fluid with fractionally charged excitations. *Phys. Rev. Lett.* **50,** 1395–1398 (1983).
3. Wen, X.-G. & Niu, Q. Ground-state degeneracy of the fractional quantum Hall states in the presence of a random potential and on high-genus Riemann surfaces. *Phys. Rev. B* **41,** 9377–9396 (1990).
4. Moessner, R. & Sondhi, S. L. Resonating valence bond phase in the triangular lattice quantum dimer model. *Phys. Rev. Lett.* **86,** 1881–1884 (2001).
5. Balents, L., Fisher, M. P. A. & Girvin, S. M. Fractionalization in an easy-axis Kagome antiferromagnet. *Phys. Rev. B* **65,** 224412 (2002).
6. Ioffe, L. B. *et al.* Topologically protected quantum bits using Josephson junction arrays. *Nature* **415,** 503–506 (2002).
7. Levin, M. & Wen, X.-G. String-net condensation: A physical mechanism for topological phases. *Phys. Rev. B* **71,** 045110 (2005).
8. Kitaev, A. Fault-tolerant quantum computation by anyons. *Ann. Phys.* **303,** 2–30 (2003).
9. Kitaev, A. Anyons in an exactly solved model and beyond. *Ann. Phys.* **321,** 2–111 (2006).
10. Jackeli, G. & Khaliullin, G. Mott insulators in the strong spin–orbit coupling limit: From Heisenberg to a quantum compass and Kitaev models. *Phys. Rev. Lett.* **102,** 017205 (2009).
11. Kim, B. J. *et al.* Phase-sensitive observation of a spin-orbital Mott state in Sr_2IrO_4. *Science* **323,** 1329–1332 (2009).
12. Leinaas, J. M. & Myrheim, J. On the theory of identical particles. *Il Nuovo Cimento* **37,** 1–23 (1977).
13. Bouwknegt, P. & Schoutens, K. Exclusion statistics in conformal field theory—generalized fermions and spinons for level-1 WZW theories. *Nucl. Phys. B* **547,** 501–537 (1999).

14. Read, N. & Rezayi, E. Beyond paired quantum Hall states: Parafermions and incompressible states in the first excited Landau level. *Phys. Rev. B* **59,** 8084–8092 (1999).
15. Slingerland, J. K. & Bais, F. A. Quantum groups and non-Abelian braiding in quantum Hall systems. *Nucl. Phys. B* **612,** 229–290 (2001).
16. Büchler, H. P., Micheli, A. & Zoller, P. Three-body interactions with cold polar molecules. *Nature Phys.* **3,** 726–731 (2007).
17. Fendley, P. Topological order from quantum loops and nets. *Ann. Phys.* **323,** 3113–3136 (2008).
18. Wheeler, J. A. Geons. *Phys. Rev.* **97,** 511–536 (1955).
19. Wheeler, J. A. On the nature of quantum geometrodynamics. *Ann. Phys.* **2,** 604–614 (1957).
20. Friedan, D., Qiu, Z. & Shenker, S. Conformal invariance, unitarity, and critical exponents in two dimensions. *Phys. Rev. Lett.* **52,** 1575–1578 (1985).
21. Cappelli, A., Itzykson, C. & Zuber, J. B. Modular invariant partition functions in two dimensions. *Nucl. Phys. B* **280,** 445–465 (1987).
22. Pasquier, V. Lattice derivation of modular invariant partition functions on the torus. *J. Phys. A* **20,** L1229–L1238 (1987).
23. Pasquier, V. Two-dimensional critical systems labelled by Dynkin diagrams. *Nucl. Phys. B* **285,** 162–172 (1987).
24. Temperley, N. & Lieb, E. Relations between percolation and colouring problem and other graph-theoretical problems associated with regular planar lattices—some exact results for percolation problem. *Proc. R. Soc. Lond. A* **322,** 251–280 (1971).
25. Feiguin, A. *et al.* Interacting anyons in topological quantum liquids: The golden chain. *Phys. Rev. Lett.* **98,** 160409 (2007).
26. Gils, C. *et al.* Collective states of interacting anyons, edge states, and the nucleation of topological liquids. *Phys. Rev. Lett.* **103,** 070401 (2009).
27. Haldane, F. D. M. 'Fractional statistics' in arbitary dimensions: A generalization of the Pauli principle. *Phys. Rev. Lett.* **67,** 937–940 (1991).
28. Freedman, M., Nayak, C. & Shtengel, K. Extended Hubbard model with ring exchange: A route to a non-Abelian topological phase. *Phys. Rev. Lett.* **94,** 066401 (2005).
29. Fradkin, E. & Shenker, S. H. Phase diagrams of lattice gauge theories with Higgs fields. *Phys. Rev. D* **19,** 3682–3697 (1979).
30. Trebst, S., Werner, P., Troyer, M., Shtengel, K. & Nayak, C. Breakdown of a topological phase: Quantum phase transition in a loop gas with tension. *Phys. Rev. Lett.* **98,** 070602 (2007).
31. Fendley, P. & Fradkin, E. Realizing non-Abelian statistics in time-reversal-invariant systems. *Phys. Rev. B* **72,** 024412 (2005).
32. Freedman, M., Nayak, C., Shtengel, K., Walker, K. & Wang, Z. A class of P,T-invariant topological phases of interacting electrons. *Ann. Phys.* **310,** 428–492 (2004).
33. Greenblatt, R. L., Aizenman, M. & Lebowitz, J. L. Rounding of first order transitions in low-dimensional quantum systems with quenched disorder. Preprint at <http://arxiv.org/abs/0907.2419v1> (2009).
34. Moore, G. & Seiberg, N. Classical and quantum conformal field theory. *Commun. Math. Phys.* **123,** 177–254 (1989).
35. Kirillov, A. N. & Reshetikhin, N. Yu. *Infinite Dimensional Lie Algebras and Groups* (ed. Kac, V. G., World Scientific, 1988).
36. Albuquerque, A. F. *et al.* The ALPS project release 1.3: Open-source software for strongly correlated systems. *J. Magn. Magn. Mater.* **310,** 1187–1193 (2007).

Acknowledgements

We thank M. Freedman, X.-G. Wen and P. Fendley for stimulating discussions. Our numerical simulations were based on the ALPS libraries[36]. A.W.W.L. was supported, in part, by NSF DMR-0706140.

Author contributions

C.G., S.T. and M.T. contributed to the numerical work. C.G., A.K., A.W.W.L and Z.W. contributed to the analytical solution. All authors contributed to the development of the general picture presented in this manuscript.

Additional information

Supplementary information accompanies this paper on www.nature.com/naturephysics. Reprints and permissions information is available online at http://npg.nature.com/reprintsandpermissions. Correspondence and requests for materials should be addressed to S.T.